Z. Phys. Chem. **222** (2008) 671–686 / **DOI** 10.1524/zpch.2008.5315
© by Oldenbourg Wissenschaftsverlag, München

Surface Analysis of Nanoscale Aluminium and Silicon Films Made by Electrodeposition in Ionic Liquids

By Fabian Bebensee[1,2], Natalia Borissenko[1], Martin Frerichs[2], Oliver Höfft[1], Wolfgang Maus-Friedrichs[2], Sherif Zein El Abedin[1,3], and Frank Endres[1,*]

[1] Faculty of Natural and Materials Science, Clausthal University of Technology, Robert-Koch-Str. 42, D-38678 Clausthal-Zellerfeld, Germany
[2] Institute for Physics und Physical Technologies, Clausthal University of Technology, Leibnizstr. 4, D-38678 Clausthal-Zellerfeld, Germany
[3] Electrochemistry and Corrosion Laboratory, National Research Centre, Dakki, Cairo, Egypt

(Received August 9, 2007; accepted September 5, 2007)

Al / Si / Nanoparticles / Electrodeposition / Ionic Liquids / XPS / HRSEM

We present a spectroscopic and microscopic study of nanoscale Al and Si films electrodeposited in water- and air-stable ionic liquids. The choice of cations for such ionic liquids has previously been shown to have a significant effect on the crystallite size of electrodeposited Al or Si films. We found that the deposits are generally uniform, dense, metallic bright, and adherent with crystallite sizes in the nanometer range. The nanocrystalline films were characterized using X-ray Photoelectron Spectroscopy (XPS) and High-Resolution Scanning Electron Microscopy (HRSEM). The XPS results show that the surface of both films is oxidized although the deposition was done in an inert gas glove box. Furthermore our results suggest that as a consequence of oxygen attack the nanoparticles are composed of a metallic core surrounded by a thin oxidic shell. Our XPS study also shows that neither the cation nor the anion of the ionic liquid is entrapped in the deposit. Thus, electrodeposition in ionic liquids delivers pure materials.

1. Introduction

The great interest in nanoscale materials is due to their unique properties (optical, electrical, magnetic, mechanical and chemical), which are mostly functions of the crystallite size of the materials. The properties of materials are strongly affected by reducing the particle size: as the particle size decreases to the nanoscale, the relative number of atoms on the grain boundary increases leading to

* Corresponding author. E-mail: frank.endres@tu-clausthal.de

dramatic effects on both, mechanical and electronic properties of the material. For example, nanocrystalline silicon showed advantages in silicon-based electronic devices due to its ability to emit light. In addition to electroluminescence, nanocrystalline silicon has unique properties such as photoluminescence and thermally induced acoustic emission. Silicon nanocrystals embedded in a SiO_2 matrix can be used for nanoscale-silicon-based laser development [1]. Nanocrystalline aluminium possesses unique mechanical properties and excellent corrosion resistance compared to microcrystalline aluminium. In a recent paper, Natter et al. [2] have observed a crystallite size dependent microhardness for nanocrystalline aluminium electrodeposited from chloroaluminate ionic liquids ranging from 1.44 GPa to 3.40 GPa for average crystallite sizes between 100 and 14 nm, respectively.

Nowadays, there is a wide variety of methods known for the preparation of nanocrystalline metals and semiconductors such as thermal spraying, sputter deposition, vapor deposition, and electrodeposition. The electrodeposition process is commercially attractive, since it can be performed at low temperatures and the experimental setup is less demanding than that one requiring ultrahigh vacuum (UHV) conditions. Furthermore, the particle size can be adjusted over a wide range by controlling the experimental parameters such as overvoltage, current density, composition, and temperature. However the question remains if electrodeposition of materials delivers materials with the purity that is achievable by physical methods. The electrodeposition of highly reactive materials (such as Al or Mg) and many semiconductors in aqueous solutions is impossible owing to the massive hydrogen evolution at the cathode. Therefore, the electrolytes must be aprotic, like organic solvents or ionic liquids.

The electrodeposition of nanocrystalline aluminium using organic solvents as electrolytes has not yet been reported. On the other hand, the electrodeposition of Al and its alloys from ionic liquids based on $AlCl_3$ was studied intensively in the past [3–23]. In a previous paper, we reported that bulk nanocrystalline aluminium can be electrodeposited from a Lewis acidic ionic liquid based on $AlCl_3$ and 1-ethyl-3-methylimidazolium chloride under galvanostatic conditions with and without nicotinic acid as a brightener [24]. Additions of nicotinic acid to the ionic liquid reduce the average crystal size from more than 100 to about 10 nm. The major disadvantage of chloroaluminate ionic liquids is their hydrolysis in the presence of water, even in traces. Therefore, they must be strictly handled under inert gas conditions. Furthermore, quite recently we have shown for the first time that nanocrystalline aluminium with an average size of the crystallites around 30 nm can be electrodeposited without any additives in the air- and water-stable ionic liquid 1-butyl-1-methylpyrrolydinium bis(trifluoromethyl sulfonyl)amide containing $AlCl_3$ [25]. However, the mechanism, why in this liquid nanomaterials are obtained is not yet completely clear. There are hints that pyrrolidinium ions are adsorbed at the electrode and crystal surfaces, thus hindering crystal growth [26]. There is no "nano-effect" if imidazolium ions are employed.

In the case of silicon, Katayama et al. have reported that a thin silicon layer can be electrodeposited from 1-ethyl-3-methylimidazolium hexafluorosilicate at 90 °C [27]. However, upon exposure to air the deposit was completely oxidized to SiO_2. It is difficult to decide whether the silicon was deposited elemental or even in a semiconducting state. In a previous paper, we have reported for the first time that semiconducting silicon can be electrodeposited in the room temperature ionic liquid 1-butyl-1-methylpyrrolidinium bis(trifluoromethylsulfonyl)amide saturated with $SiCl_4$. The investigations were performed on highly oriented pyrolytic graphite (HOPG), and a silicon layer with a thickness of 100 nm exhibiting a band gap of 1.0 ± 0.2 eV was obtained [28]. We have also shown a detailed in situ Scanning Tunneling Microscopy (STM) study of silicon electrodeposition onto Au(111) using the above mentioned ionic liquid with a lower concentration of $SiCl_4$(0.1 M). A silicon layer with a thickness of about 5 nm was found to be semiconducting with a symmetrical band gap of 1.1 ± 0.2 eV [26].

In the present paper, nanocrystalline aluminium and silicon were electrodeposited from the water- and air-stable ionic liquid 1-butyl-1-methylpyrrolidinium bis-(trifluoromethylsulfonyl)amide on Si(100) and stainless steel substrates, respectively. Both materials are highly reactive and covered per se by a thin oxide layer. Apart from the surface oxidation we were interested if the ionic liquid or any ion is incorporated into the material during electrodeposition. XPS is one of the few methods which is sensitive enough to probe even low amounts of impurities. Thus, the deposits were characterized using X-ray Photoelectron Spectroscopy (XPS) and High-Resolution Scanning Electron Microscopy (HRSEM). Our investigations indicate a core-shell-structure of the crystallites. This deposition route enables the facile preparation of nanocrystalline aluminium and silicon films, which offer promise for fabrication of chemically responsive materials.

2. Experimental

2.1 Preparation of the deposits

The ionic liquid 1-butyl-1-methylpyrrolidinium bis(trifluoromethylsulfonyl)amide (Merck/EMD) was purchased in the highest available (ultrapure) quality. For simplicity, the name of the ionic liquid is abbreviated according to the main components, in this case [BMP]Tf_2N. For purification, the ionic liquid was dried under vacuum and stirring conditions for 12 hours at a temperature of 100 °C to a water content below 3 ppm (by Karl-Fischer titration) and stored in an argon filled glove box with water and oxygen contents below 2 ppm (OMNI-LAB from Vacuum Atmospheres). Additionally performed cyclo-voltammograms on Pt give no evidence for electrochemically active water.

Anhydrous $AlCl_3$ (Fluka, 99 %) and $SiCl_4$ (Alfa Aesar, 99.999 %) were used as sources of Al and Si, respectively. The electrochemical cell was made of

polytetrafluoroethylene and clamped over a Teflon covered Viton o-ring onto the substrate yielding a geometric surface area of either 0.28 cm^2 or 0.79 cm^2 for the samples analysed by XPS. The deposition was performed in a glove box using a Parstat 2263 Potentiostat/Galvanostat (Princeton Applied Research) controlled by PowerCV and PowerStep software. A solution of about 1 M $SiCl_4$ in [BMP]Tf_2N was used for the deposition of the Si films. The mixture of [BMP]Tf_2N with $AlCl_3$ shows biphasic behaviour in the concentration range from 1.6 to 2.5 mol/l. At elevated temperatures beyond 80 °C, the mixture becomes monophasic [25]. For deposition at room temperature, only the upper phase was used since Al cannot be deposited from the lower phase. The aluminium films were prepared potentiostatically at a potential of −1.4 V (vs. Al/$AlCl_3$) for two hours. The silicon films were prepared potentiostatically, too, at a potential of −1.7 V (vs. Pt quasi reference electrode) for two hours. For details on the electrochemistry of $SiCl_4$ and of $AlCl_3$ in these liquids we would like to refer to our original publications [26, 29]. If not otherwise stated all experiments were performed at room temperature (~ 23 °C).

2.2 Preparation of the samples

Substrates were Si(100) single crystals (for Al deposition) or stainless steel plates (for Si deposition). Various sample-materials were tested before choosing the most practicable ones for both deposits. Si(100) was chosen for the Al deposition, since it is a widely used substrate in surface science and no alloying is known for the Si/Al-system. In the case of silicon, a stainless steel sample holder was coated directly. Especially for the following analysis it was important to use a substrate material which can be easily distinguished from the deposits. Thus, stainless steel was the best compromise.

Prior to electrodeposition, the substrates were intensively cleaned and dried. Additionally, the Si(100) samples were etched and hydrogenated with HF which simplifies the following deposition of aluminium [30]. After deposition all samples were cleaned in the argon-filled glove box with acetonitrile to remove the ionic liquid as well as possible. We would like to point out clearly that all handling was done in the glove box, thus the samples were not exposed to air.

2.3 Spectroscopic and microscopic measurements

A High Resolution Scanning Electron Microscope (HRSEM) (Carl Zeiss DSM 982 Gemini) was utilized to investigate the surface morphologies. Particle sizes are determined from these images. A detailed analysis of Al grain size distribution with Scherrer and Warren-Averbach analysis can be found in [29]. The atomic composition and oxidation states of the Al and Si were studied by X-ray Photoelectron Spectroscopy (XPS) using an OMICRON NG DAR 400. For both material types spectra were recorded under UHV conditions (10^{-10} mbar), using Al K_α primary radiation (14 kV, 20 mA, 1486.6 eV). After acquisition of the spectra, various data handling procedures were carried out on the raw data. Survey (broad energy range, low resolution) spectra were collected to determine the elemental composition of the sample surfaces. High resolution spectra (resolution of 0.6 eV) of the Si 2p and Al 2p core levels were collected to determine chemical/bonding states. All given values in eV are referenced to the C 1s peak (in this case C 1s = 287 eV). XPS is a highly surface sensitive technique, providing information on the outermost 5–10 nm of the sample. After preparation in the argon-filled glove box, the samples were attached onto the sample holder with double-side adhesive tape and transferred to an argon filled transfer chamber which was afterwards attached to the fast-entry chamber of the UHV apparatus. XPS peaks were fitted mathematically using overlapping Gauss profiles. The fitting was performed applying OriginPro7 including the Peak Fitting Module (OriginLab Corporation). The full width at half maximum (FWHM) and the position of the Si 2p and Al 2p peaks were obtained in previous measurements (not shown here) and are used as fitting parameters in order to get more reliable fitting results.

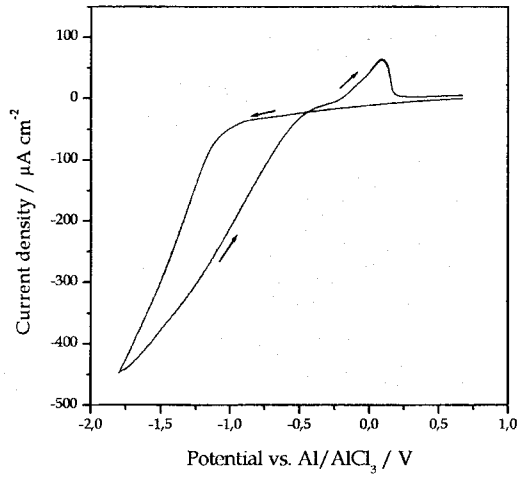

Fig. 1. Cyclic voltammogram of the ionic liquid 1-butyl-1-methylpyrrolidinium bis(trifluoromethyl-sulfonyl)amide containing 1.6 M $AlCl_3$ on Si(100) substrate (upper phase of the biphasic liquid).

3. Results and discussion

3.1 Aluminium

Fig. 1 shows the cyclic voltammogram of the upper phase of the biphasic mixture of 1.6 M $AlCl_3$/[BMP]Tf_2N on Si(100) at room temperature. The electrode po-

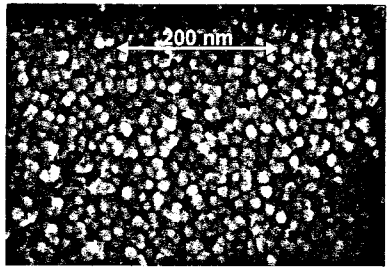

Fig. 2. High Resolution Scanning Electron Microscopy (HRSEM) image of the aluminium nanocrystallites on Si(100).

tential was scanned from the open circuit potential in the negative direction at a rate of 10 mVs^{-1}. The onset of the bulk deposition on Si(100) occurs at a potential of about −1.5 V. In the reverse scan, the anodic scan intersects with the cathodic one indicating that the deposition of Al onto Si(100) requires an overpotential to initiate the nucleation and growth of the bulk deposit. The peak observed in the anodic branch of the cyclic voltammogram is due to the partial stripping of the aluminium deposit. At room temperature, the electrodissolution of Al on Si(100) is not complete in this ionic liquid as on other substrates, too.

Fig. 2 displays a High Resolution Scanning Electron Microscopy (HRSEM) picture of the aluminium sample. The particles exhibit sizes of approximately 16 nm ± 3 nm and constitute a film covering the silicon substrate completely. The film thickness of the deposits is approximately 1 μm. This result is similar to our previous results with Au(111) and glassy carbon as substrates.

Recently we have reported that the $[BMP]^+$ cation might be adsorbed on the surface and on growing Al nuclei, thus hindering the further growth of Al crystallites, leading to nanosized deposits [29]. It is still unclear up to now to which extent the Tf_2N anion is co-adsorbed and contributes to formation of nanocrystallites. MacFarlane et al. [31] have described that the Tf_2N anion is subject to some irreversible cathodic breakdown.

The reduction of Tf_2N weakens one of the N-S bonds leading to its cleavage [31]:

$$N(SO_2CF_3)_2^- + e^- = N(SO_2CF_3)_2^{2-} = {}^{\bullet}NSO_2CF_3^- + SO_2CF_3^- \quad (1)$$

The reduction products of Tf_2N can undergo further reduction reactions as follows:

$${}^{\bullet}NSO_2CF_3^- + e^- = NSO_2^- + CF_3 \quad (2)$$

$$SO_2CF_3^- + e^- = SO_2^- + CF_3^- \quad (3)$$

If we perform the Al deposition in the ionic liquid 1-Ethyl-3-methylimidazolium bis(trifluoromethylsulfonyl)amide ($[EMIm]Tf_2N$), we get microcrystalline deposits [29]. This leads us to the conclusion that adsorption of the $[BMP]^+$ cation

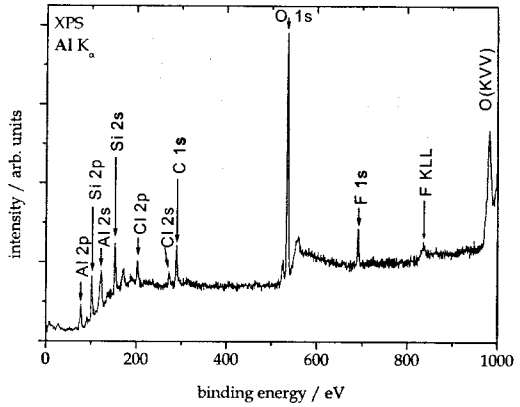

Fig. 3. Survey XPS spectrum of an aluminum nanoparticle film on Si(100).

is responsible for the formation of nanosized deposits. We have currently no hint that Tf_2N-breakdown occurs during Al deposition in $[BMP]Tf_2N$. Thus we exclude that the nanostructure of the deposit is induced by Tf_2N-breakdown as it was mentioned to us.

Fig. 3 shows a XPS survey spectrum with a binding energy range from 0 to 1000 eV of an aluminium covered Si(100) sample. The aluminium film was prepared potentiostatically at an electrode potential of −1.4 V (vs. $Al/AlCl_3$ reference electrode) for two hours in the upper phase of the biphasic mixture $[BMP]Tf_2N/1.6$ mol/l $AlCl_3$. The intensity is plotted as a function of the binding energy. All relevant peaks are labelled with the corresponding element. This spectrum is representative of all Al surfaces obtained during our experiments. On the Al films we found additional components like chlorine, carbon, oxygen, and fluorine, which mostly could be assigned to a contaminating layer (residues of the ionic liquid and $AlCl_3$) on top of the samples. Part of the oxygen amount has to be caused by the atmosphere of the inertgas glove box, too. Just the Si peaks are due to the substrate. In addition to the spectra shown here, XP spectra were recorded after samples have been sputtered using Ar ions for different (increasing) time spans. The spectra indicated that the oxygen content of the sample decreased initially before reaching a nearly constant level. The additional components like chlorine and fluorine are almost not detectable after sputtering, thus we can exclude that the ionic liquid is incorporated in the deposits.

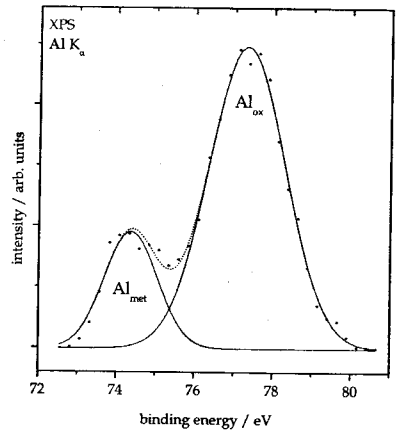

Fig. 4a. High resolution XPS spectrum of an aluminium nanoparticle film on Si(100) (Dots: Original Data obtained from the measurement, Solid Lines: Fitted Data, Dotted Line: sum of both fitted contributions).

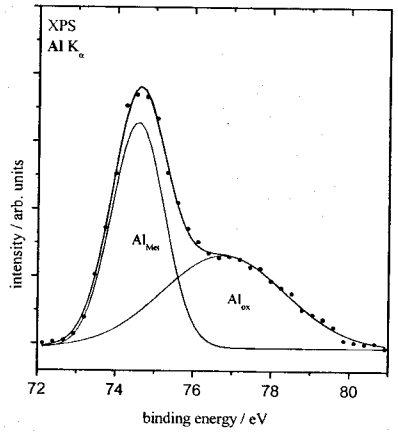

Fig. 4b. High resolution XPS spectrum of the sputtered aluminium nanoparticle film on Si(100) (Dots: Original Data obtained from the measurement, Solid Lines: Fitted Data, Dotted Line: sum of both fitted contributions).

Fig. 4a displays a high resolution spectrum (resolution of 0.6 eV; all values in eV relative to C 1s = 287 eV) of the Al 2p peak. The feature at a binding energy of 74.4 eV (Al_{met}) exhibits a FWHM of 1.6 eV while the feature at a binding energy of 77.3 eV (Al_{ox}) shows a FWHM of 2.3 eV. The presence of

the two features indicates that the Al occurs at least in two different oxidation states [32]. Fig. 4b shows a high resolution spectrum of the Al 2p peak after 20 min. sputtering with Ar Ions. The above mentioned two features are present too, but there is a strong change in the intensity of the peaks.

The results shown in the previous section indicate that Al is present in two different oxidation states. The feature with higher binding energy in the Al 2p peak can be attributed to oxidized Al (Al^{3+}), the feature at lower binding energy emerges from metallic Al [32–35]. A small amount of (Al^{3+}) bound in $AlCl_3$ at the surface cannot be excluded at this point. The sputter results (see discussion below) showed clearly that $AlCl_3$ can only be found in the contamination layer. To calculate the thickness of an oxide layer on top of a metallic layer the following formula can be applied:

$$d = \lambda \cdot \cos(\vartheta) \cdot \ln\left(\frac{D_{met} \cdot \lambda_{met} \cdot I_{ox}}{D_{ox} \cdot \lambda_{ox} \cdot I_{met}} + 1\right) \text{ [33, 34]} \quad (4)$$

with d being the thickness of the oxide layer in Å, ϑ the angle between the surface normal and the axis of the analyzer, D the density of the Al or Si atoms in the pure or oxidized material, λ the inelastic mean free path in Å, I the intensity (measured by integration of the area under the curve). The indices indicate the oxidized (ox) or the metallic (met) species, respectively. Determination of layer thicknesses by comparison of spectra recorded before and after the preparation of the layer is quite simple using the exponentially dampened signal of the substrate. Here, the ratios of the oxidized and metallic species are used as a measure for this dampening facilitating layer thickness determination without comparing the spectrum of the substrate with that of the prepared layer on the substrate.

Applying Eq. (4) to the XP spectra of the Al nanoparticles before sputtering yields an oxide layer thickness of approximately 4 nm. However, as for geometric reasons the Al particles can not be handled as planar layers (as required for the model, Eq. 4), this value describes an upper limit for the oxide layer thickness. In an ultra high vacuum (UHV) experiment the thickness of an Al oxide layer is limited to a maximum value of 2.1 nm [33]. After sputtering the oxide layer thickness is in the range of the value of the UHV experiment. It seems reasonable that the nanocrystallites particularly in the surface of the Al-film exhibit oxide layer thicknesses that are above this value, since the oxide layer is not formed under UHV conditions but rather in the atmosphere of the inertgas glove box. The amount of oxygen in the atmosphere of the glove box is $1 \cdot 10^{-3}$ mbar, this corresponds to an exposure of $1 \cdot 10^{6}$ L (Langmuir; 1 L = $1 \cdot 10^{-6}$ Torr s) O_2 during the whole of the experiment. This exposure is sufficient to explain the oxide layer thicknesses, compared to the UHV experiments [33]. An oxidation by the ionic liquid itself can be excluded at this point, because the [Tf_2N] anion is very stable and we did not find any residues of the ionic liquid especially of the anion in deeper layers of the film. But the solubility of O_2 in [BMP]Tf_2N of 6.1 mM [36] indicates that the oxidation could start after

the electrodeposition was completed. We cannot exclude an influence of chloride from $AlCl_3$ on the oxidation process like in aqueous solution until now. This has to be subject of further studies with Al complexes without chlorine, e.g. $Al(Tf_2N)_3$. Furthermore we have to take into account that the cleaning process with acetonitrile and the residence time of the film in the glove box contributes to the oxidation, too.

In addition the spectra of the sputtered film indicated that the oxygen content of the sample reaches a nearly constant level after sputtering. It is therefore concluded, that the crystallites constiute a film which is porous enough for oxygen to penetrate into the bulk portion of the film, even in the inertgas glove box.

It is an important result that nearly no residues of the ionic liquid and the $AlCl_3$ could be found in deeper layers of the film. Thus electrodeposition in ionic liquids is a clean procedure.

The intensity of the aluminium peak of the not sputtered film (Fig. 4a) might be perceived as rather small, especially compared to the rather pronounced oxygen-peak displayed in the survey spectrum. This has mainly two reasons: the cross section of oxygen and therewith the count rate is much larger than the cross section of aluminium. Secondly, the area covered by the deposit is smaller than the analysed area, which also accounts for the presence of the silicon peaks in the survey spectrum. As the thickness of the deposit is in the order of one micrometer, contributions from the substrate underneath the deposit are clearly excluded.

The morphological information obtained from the HRSEM micrograph, which was acquired using secondary electrons as the signal, was evaluated to determine the average crystallite size. This was achieved by manually measuring a significant number of crystallites.

The combination of the results from the XPS measurements with those obtained from the HRSEM image implies that the Al particles exhibit a core-shell structure, with a metallic core surrounded by an oxide shell as a result of some oxygen attack, even under inert gas. The particles have diameters of about (16 ± 3) nm with a rather narrow size distribution. The oxide shell is making up a maximum of 8 nm of the particle diameter. It is remarkable that even in the inert atmosphere of an argon filled glove box aluminium is rapidly oxidized at the surface. From materials aspects an in situ passivation routine for aluminium in ionic liquids has to be developed to keep a metallic material.

3.2 Silicon

As shortly reported in the introduction silicon is quite an important semiconductor. We were the first ones who showed by in situ tunnelling spectroscopy (see [26]) that silicon can be electrodeposited in ionic liquids as element and that under in situ electrochemical conditions the typical band gap of silicon can be determined. Nevertheless sometimes it happened that the electrochemically made

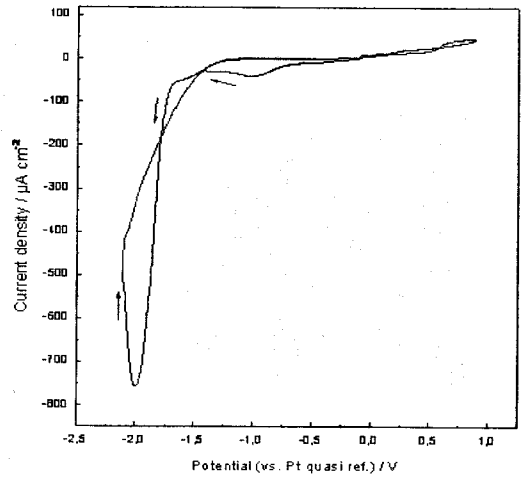

Fig. 5. Cyclic voltammogram of the ionic liquid 1-butyl-1-methylpyrrolidinium bis(trifluoromethylsulfonyl)amide containing 1 M $SiCl_4$ on stainless steel electrode.

Si was completely oxidized under air, sometimes there was hardly any oxidation (just from EDX-results). As surface oxides or defects in silicon might alter the properties considerably it was our aim to investigate to which extent the electrochemically made silicon is subject to oxidation if made under the best available conditions, i.e. under inertgas ($O_2 < 2$ ppm) and UHV.

Fig. 5 shows the cyclic voltammogram of the ionic liquid 1-butyl-1-methylpyrrolidinium bis(trifluoromethylsulfonyl)amide containing 1 M $SiCl_4$ on stainless steel electrode. The electrode potential was scanned from the open circuit potential (-0.3 V vs. Pt.) in the negative direction at a scan rate of 10 mVs^{-1}. The reduction peak observed in the forward scan at a potential of -1.0 V is maybe correlated to the formation of Fe/Si surface alloy. The onset of bulk deposition of Si starts at a potential of about -1.7 V. In the reverse scan, no oxidation peak was recorded indicating the irreversibility of this system.The electrodeposition experiments have been carried out potentiostatically at potentials slightly more negative than the deposition potential of Si for 2 hours. The Pt quasi reference electrode is only a compromise as there is no reversible redox process. However, if the platinum wire is heated in a hydrogen flame before, it delivers in all experiments more or less the same relative electrode potential so that we can use Pt wires reliably enough as (quasi-) reference electrodes. The Si deposition on stainless steel is quite similar to deposition on other substrates that we have investigated before (HOPG, Au(111), glassy carbon).

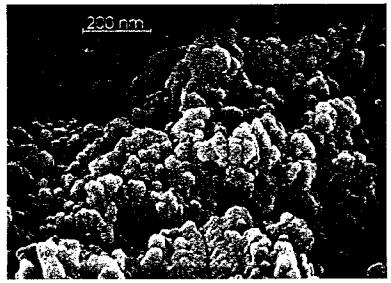

Fig. 6. High Resolution Scanning Electron Microscopy (HRSEM) image of the nanoscale silicon.

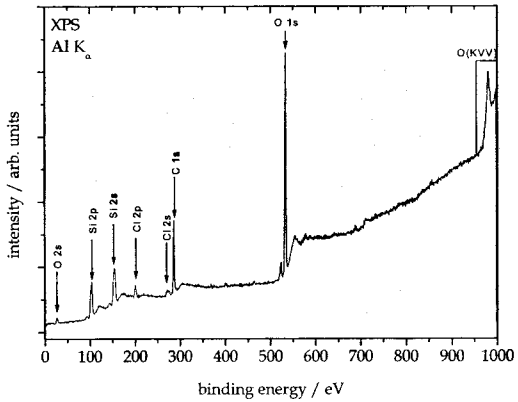

Fig. 7. XPS spectrum of a silicon nanoscale film on a steel sample.

Fig. 6 displays a High Resolution Scanning Electron Microscopy image of the deposited nanoscale silicon. The particles cover the substrate completely and exhibit sizes of (36 ± 9) nm. This particle size is beyond the size where quantum confinement has to be expected (~ 5 nm) but supports our hypothesis that in liquids with the BMP^+-cation rather nanosized deposits are obtained. Compared to the aluminium particles, they seem to form a much more porous structure. Furthermore there seems to be a connection between the particles which is not surprising at all: in contrast to a metallic structure carbon, silicon and germanium are sp^3-bound materials. Thus, a particle is either surface terminated (e.g. by chloride or Tf_2N) or bound chemically to another particle. Using this electrodeposition route we can get film thicknesses in the micrometer range. The films investigated here exhibited film thicknesses of about 1 µm.

Fig. 7 shows a XPS survey spectrum of a stainless steel substrate covered with a Si nanoparticle film. Again, this spectrum is representative of all Si films

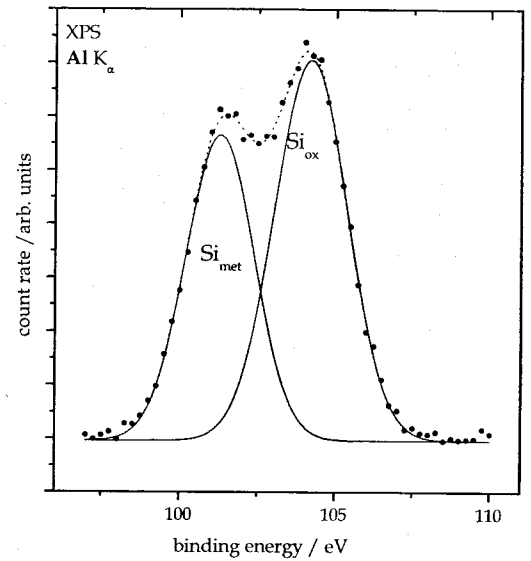

Fig. 8. High resolution XPS spectrum of a nanoscale silicon film on a stainless steel substrate (Dots: Original Data obtained from the measurement, Solid Lines: Fitted Data, Dotted Line: sum of both fitted contributions).

obtained during our experiments. Besides the Si 2s and 2p features, there are some obvious features of other elements: carbon, oxygen and chlorine. As mentioned above, these elements are due to a thin contamination layer, presumably originating from the ionic liquid, the solvent and the atmosphere of the glove box. Interestingly, in contrast to aluminum no fluorine was detected with XPS, even at the surface.

The high resolution spectrum (resolution of 0.6 eV; all values in eV relative to C 1s = 287 eV) of the Si 2p peak displayed in Fig. 8 reveals that the peak (as in the case of Al) contains two contributions. The Si 2p features show binding energies of 101,3 eV (Si_{met}) and 104,4 eV (Si_{ox}) and a FWHM of 2.6 eV and 2.8 eV, respectively. Similar to the Al film, it is likely to assume that these XPS features are due to at least two different oxidation states of the silicon.

Similar to the XPS results for Al, Si is also present in at least two different oxidation states as is indicated by the two features in the high resolution XPS spectrum. The two contributions of the Si 2p peak can be attributed to elemental Si and SiO_x, respectively. The measured differences in the binding energies between the O 1s and the elemental Si 2p peak (432.3 eV) as well as between the O 1s and the SiO_x 2p peak (429.4 eV) are consistent with the corresponding values obtained by Hollinger [37] (429.5 eV and 433.0 eV, respectively). We cannot rule out that some of the silicon is terminated with chlorine, because for

example the values for Si^{3+} in $SiCl_3$ are in the same range like the values for Si in SiO_x [37, 38].

The formula used for the calculation of the oxide layer thickness introduced above (see Eq. 4) can also be applied to determine the thickness of the SiO_x layer. The resulting layer thickness of 8 nm is only to be seen as an upper limit, because, again, the formula was derived for planar geometries and not for rather round particles. In any case these XPS studies show without doubt that electroreduction of $SiCl_4$ in [BMP]Tf_2N leads to elemental silicon without any hint for incorporation of the ionic liquid or any of its ions. As discussed in the case of Al the electrochemically made silicon is subject to some surface oxidation due to oxygen content in the glove box. Thus, for a technological process an in situ passivation in the ionic liquid would have to be developed. In any case our results show without doubt that the electrodeposition of Si initially delivers a chemically pure and clean material.

4. Summary

We have presented our first surface analysis results of electrodeposited nanocrystalline Al and nanoscale Si films with crystallite sizes in the nanometer range using the air- and water-stable ionic liquid 1-butyl-1-methylpyrrolidinium bis(trifluoromethylsulfonyl)amide ([BMP]Tf_2N). In addition to the air- and water-stability, the employed ionic liquid exhibits some interesting properties: it is easy to dry to water contents below 3 ppm and has a wide electrochemical window of about 5 V. This enables the electrochemical production of (nano-)materials which formerly could only be made by physical methods. Generally, the deposits obtained are initially uniform, dense, metallic bright, and adherent. The residual ionic liquid can be washed from the electrochemically made samples with acetonitrile under inert gas atmosphere. After transferring the sample from the inert gas to UHV, the chemical composition of the films was investigated by XPS and the surface morphology was determined independently by HRSEM. The XPS measurements suggest that both the Al and the Si are only partly oxidized forming a structure with a metallic core and an oxide shell. The oxide layer thickness was calculated semiquantitatively by detailed analysis of the Al 2p and the Si 2p peaks, respectively. For aluminium an oxide layer of 4 nm and for silicon an oxide layer of 8 nm of maximum thickness was found. The particle sizes were determined to be (36 ± 9) nm for Si and (16 ± 3) nm for Al. The present study not only shows that both, Si and Al can be made as nano-sized material by electrodeposition from ionic liquids, but also demonstrates the successful transfer of the electrochemically made samples to UHV conditions for further analysis without exposing them to ambient conditions. Furthermore ionic liquids are obviously not incorporated during electrodeposition.

Acknowledgement

Financial support by the German Research Foundation (DFG) is gratefully acknowledged. We thank Dr. Anissa Gömann for experimental support with the XPS measurements.

References

1. S. L. Jaiswal, J. T. Simpson, S. P. Withrow, C. W. White, and P. M. Norris, Appl. Phys. A. **77** (2003) 57.
2. H. Natter, M. Bukowski, R. Hempelmann, S. Zein El Abedin, E. M. Moustafa, and F. Endres, Z. Phys. Chem. **220** (2006) 1275.
3. R. T. Carlin, R. A. Osteryoung, and J. Electrochem, Soc. **136** (1989) 1409.
4. M. R. Ali, A. Nishikata, and T. Tsurut, Ind. J. Chem. Tech. **6** (1999) 317–324.
5. M. Lipsztajn, R. A. Osteryoung, and J. Electrochem, Soc. **130** (1983) 1968.
6. P. K. Lai, M. Skyllas-Kazacos, and J. Electroanal, Chem. **248** (1988) 431.
7. G. R. Stafford and J. Electrochem, Soc. **136** (1989) 635.
8. S. Takahashi, K. Akimoto, and I. Saeki, Hyomen Gijutsu **40** (1989) 134.
9. T. J. Melton, J. Joyce, J. T. Maloy, J. A. Boon, and J. S. Wilkes, J. Electrochem. Soc. **137** (1990) 3865.
10. A. Shibuya, J. Uchida, Y. Yamamoto, H. Seto, and T. Tsuda, Mater. Sci. Forum **577** (1991) 73–75.
11. C. Scordilis-Kelly, J. Fuller, and J. S. Wilkes, J. Electrochem. Soc. **139** (1992) 694.
12. G. M. Janovski and G. R. Stafford, Metall. Trans. A. **23** (1992) 2715.
13. T. P. Moffat, G. R. Stafford, and D. E. Hall, J. Electrochem. Soc. **140** (1993) 2779.
14. T. P. Moffat, J. Electrochem. Soc. **141** (1994) L115.
15. G. R. Stafford, J. Electrochem. Soc. **141** (1994) 245.
16. Y. Zhao and T. J. VanderNoot, Electrochim. Acta **42** (1997) 1639.
17. T. Takenaka and M. Kawakami, Int. J. Mater. Prod. Technol. **2** (2001) 500.
18. T. Tsuda, C. L. Hussey, G. R. Stafford, and J. E. Bonevich, J. Electrochem. Soc. **150** (2003) C243.
19. B. J. Welch and R. A. Osteryoung, J. Electrochem. Soc. **118** (1981) 455.
20. Q. Liao, W. R. Pitner, G. Stewart, and C. L. Hussey, J. Electrochem. Soc. **144** (1997) 936.
21. T. Tsuda, C. L. Hussey, and G. R. Stafford, J. Electrochem. Soc. **151** (2004) C379.
22. M. R. Ali, A. Nishikata, and T. Tsurut, Electrochimica Acta **42** (1997) 2347.
23. M. Matsunaga, T. Kitazaki, K. Hosokawa, S. Hirano, and M. Yoshida, *Molten Salts. The Electrochemical Society Proceedings Series*. Pennington, NJ (1994).
24. F. Endres, M. Bukowski, R. Hempelmann, and H. Natter, Angew. Chem. **115** (2003) 3550.
25. S. Zein El Abedin, E. M. Moustafa, R. Hempelmann, H. Natter, and F. Endres, Electrochem. Comm. **7** (2005) 1116.
26. N. Borisenko, S. Zein El Abedin, and F. Endres, J. Phys. Chem. B **110** (2006) 6250–6256.
27. Y. Katayama, M. Yokomizo, T. Miura, and T. Kishi, J. Electrochem. **69** (2001) 834.
28. S. Zein El Abedin, N. Borissenko, and F. Endres, Electrochem. Comm. **6** (2004) 510.
29. S. Zein El Abedin, E. M. Moustafa, R. Hempelmann, H. Natter, and F. Endres, ChemPhysChem **7** (2006) 1535.
30. K. Oura, V. G. Lifshits, A. A. Saranin, A. V. Zotov, and M. Katayama, Surf. Sci. Rep. **35** (1999) 1–69.

31. P. C. Howlett, E. Izgorodina, M. Forsyth, and D. R. MacFarlane, Z. Phys. Chem. **220** (2006) 1483.
32. M. Frerichs, F. Voigts, and W. Maus-Friedrichs, Appl. Surf. Sci. **253** (2006) 950–958.
33. B. R. Strohmeier, Surf. Int. Anal. **15** (1990) 51–56.
34. E. McCafferty and J. P. Wightman, Surf. Int. Anal. **26** (1998) 549–564.
35. T. Kravchuk, R. Akhvlediani, V. V. Gridin, and A. Hoffmann, Surf. Sci. **562** (2004) 83–91.
36. R. G. Evans, O. V. Klymenko, S. A. Saddoughi, C. Hardacre, and R. G. Compton, J. Phys. Chem. B **108** (2004) 7878–7886.
37. G. Hollinger, Appl. Surf. Sci. **8** (1981) 318–336.
38. C. K. Oh, S. D. Park, H. C. Lee, J. W. Bae, and G. Y. Yeom, Electrochem. Solid-State Lett. **10** (2007) H94–97.